Amplitude and phase changes for reflected and transmitted waves from a curved interface in anisotropic media

Bjørn Ursin, Nathalie Favretto-Cristini, Paul Cristini

submitted to *Geophys. J. Int.*

Amplitude and phase changes for reflected and transmitted waves from a curved interface in anisotropic media

Bjørn Ursin[1⋆], Nathalie Favretto-Cristini[2†] and Paul Cristini[2‡]

[1] *Norwegian University of Science and Technology (NTNU), Department of Electrical Systems, O.S.Bragstads Plass 2B, 7491 Trondheim, Norway*

[2] *Aix-Marseille Univ, CNRS, Centrale Marseille, LMA, Marseille, France*

SUMMARY

It is well known that seismic data that have been recorded in complex geological environments must be compensated for geometrical spreading before AVO/AVA analysis, in order to avoid erroneous imaging interpretation. By investigating analytically both the effect of the geometrical spreading and the effect of the reflector curvature on amplitude and phase changes for reflected and transmitted waves between anisotropic media, using ray theory, we show that these data should be compensated for interface effects as well. In order to gain insight more specifically in the focusing effect of the interface, the special case of homogeneous isotropic media separated by a curved interface of syncline type is discussed and compared to the case of a plane interface. 3D numerical simulations of wave reflection from curved interfaces using a Spectral-Element Method validate our analytical derivations. In particular, numerical seismograms obtained at a vertical receiver array highlight that the effect of interface curvature on the reflected events is much more pronounced in a restricted area associated with the existence of caustics, which is consistent with our analytical predictions. Moreover, comparisons between the numerical and the analytical results

confirm the fact that using plane-wave reflection coefficients without correction for the interface effect may lead to wrong interpretation of AVA/AVO analysis.

Key words: Body waves, computational seismology, seismic anisotropy, wave propagation

1 INTRODUCTION

Complex geological structures present significant challenges in imaging and interpretation of seismic data for exploration applications. Their geometrical characteristics (*e.g.,* curved interfaces) and physical properties (*e.g.,* anisotropy, heterogeneities) may cause significant distortions of seismic wavefronts and amplitudes (Gjøystdal et al., 1984; Maultzsch et al., 2003; Xu et al., 2005), making for instance AVO (amplitude-versus-offset) or AVA (amplitude-versus-angle) analysis challenging (Skopintseva et al., 2012). In order to avoid misleading amplitudes and phases, and therefore significant imaging errors and erroneous geologic interpretation, it is well known that seismic data must be compensated for geometrical spreading before AVO/AVA analysis (Xu & Tsvankin, 2006). They should be compensated for interface effects as well. The purpose of this paper is to investigate the effects of the interface curvature on amplitude and phase changes for reflected and transmitted waves between anisotropic media.

Previous papers have partially addressed these issues, most of them in the context of ray theory, since conventional AVO/AVA inversion mainly relies on ray-based approaches to describe the reflection/transmission phenomena. For instance, Ursin (1986) has used dynamic (paraxial) ray theory to compute the reflection response from a curved surface between isotropic media for zero-offset configuration. Brandsbergh-Dahl et al. (2003), and later on Koren & Ravve (2011) and Ravve & Koren (2011), have computed reflection responses from a single-dipping reflector in 3D heterogeneous anisotropic media. However, the responses are not corrected for reflector curvature effects. Červený et al. (1974), Hubral (1979), and later on Hubral et al. (1995) have derived equations for how the geometrical spreading for propagating waves depends, within the high-frequency approximation, on interface curvature. The most straightforward way to compute geometrical spreading for waves propagating in anisotropic media is by performing dynamic ray tracing (Schleicher et al., 2001). However, alternative

⋆ bjorn.ursin@ntnu.no
† favretto@lma.cnrs-mrs.fr (Corresponding author)
‡ cristini@lma.cnrs-mrs.fr

approaches, more suitable for AVO processing, and based for instance on expressions of geometrical spreading using measured traveltimes of primary reflection events from horizontal interfaces, have also been proposed in (Zhou & McMechan, 2000; Ettrich et al., 2002; Ursin & Hokstad, 2003; Xu et al., 2005; Xu & Tsvankin, 2006) (see also the references given there). The Tau-p transform is known to be one of the best ways to correct for geometrical spreading in laterally homogeneous media separated by a flat interface (van der Baan & Smit, 2006). Zhu & McMechan (2015) have explored the applicability and effectiveness of the 2D Tau-p transform when the subsurface model includes heterogeneous overburden and/or curved interfaces (of anticline type). Thanks to sensitivity studies, they have shown that the Tau-p transform is still effective only for overburdens with weak heterogeneities (*e.g.*, vertically smoothly varying properties or transversely isotropic properties) and only for weakly curved reflectors. More importantly, they have pointed out that the effect of interface curvature is predominant compared to that of the overburden. In this context, it makes sense to focus our work more specifically on the effect of interface curvature on geometrical spreading and on the characteristics of the reflected and transmitted waves. Note that the approach described in (Zhu & McMechan, 2015) is 2D and extending it to 3D may be relatively difficult.

Besides the effect on geometrical spreading, the reflector geometry can have a more direct effect on the reflectivity response of the interface. In AVO/AVA analysis the amplitude of a reflected wave is often modelled as a reflection coefficient corrected for geometrical spreading and a possible phase shift due to caustics. The most common approach is to rely on a strong assumption (namely, the wave is reflected by a locally plane interface), and hence to use the exact or linearized plane-wave reflection coefficient for elastic isotropic media (*e.g.*, (Castagna, 1993; Ursin & Tjåland, 1996; Aki & Richards, 2002; Avseth et al., 2005)). Extensions have been derived for elastic anisotropic media by (Chapman, 1994; Ursin & Haugen, 1996), and for anelastic anisotropic media by (Stovas & Ursin, 2003; Carcione, 2015). In the near field of a point source, as the incident wavefront is not plane, it is necessary to replace the plane-wave reflection coefficient by a frequency-dependent spherical-wave reflection coefficient (*e.g.*, (Červený & Hron, 1961; Ursin & Arntsen, 1985)). Harrison & Nielsen (2004) have shown that plane-wave reflection coefficients and spherical-wave reflection coefficients are related by a Hankel transform. AVO and data inversion using spherical-wave reflection coefficients have been demonstrated successful (Alhussain et al., 2008; Zhu & McMechan, 2015; Yan et al., 2020). However, it has to be remembered that, although they are largely used in common AVO/AVA studies, plane-wave reflection coefficients and spherical-wave reflection coefficients are strictly valid only for plane reflectors. Ayzenberg et al. (2009) have then derived

a generalization of plane-wave reflection coefficients that accounts for interface curvature, namely the effective reflection coefficients. Skopintseva et al. (2012) have demonstrated the effectiveness of effective reflection coefficients for AVO inversion of near- and post-critical reflections. However, the choice of the appropriate reflection/transmisison coefficients (plane-wave, spherical-wave, effective) is a trade-off between computational cost/speed and quality/accuracy. For instance, Favretto-Cristini et al. (2017) have shown that, depending on the interface geometry (curvature, slope...), considering effective reflection coefficients may lead to large computational costs and is not mandatory to reach a largely acceptable accuracy of the results. In this context, we consider plane-wave reflection coefficients in our work here, since these reflection coefficients are still currently the most used in AVO/AVA inversion. Moreover, for the specific case of vertical seismic profiles (as considered in the illustrative part of this paper), the reflector curvature may locally be considered as plane, and therefore effective, spherical-wave and plane-wave reflection coefficients are more or less similar.

Despite the numerous works on the geometrical spreading and on the effective reflectivity of interfaces reported in literature, to our best knowledge, no paper has studied so far explicitly the influence of both the geometrical spreading and the interface curvature on the wave characteristics, and more specifically the induced focusing/defocusing effect. This is the goal of our work here.

Ray methods play a significant role in seismic modelling, seismic traveltime inversion, and seismic imaging. In particular, dynamic ray tracing is widely used to compute the reflection response from an interface, and to compute the geometrical spreading factor of the zeroth-order ray-theory solution (or high-frequency Green function) of an elementary seismic wave which propagates from a source to a receiver. In the work presented here, we also use ray theory to establish the reflected/transmitted wave response (in terms of amplitude and phase) from a curved interface between anisotropic media. Therefore, some recalls on ray tracing in anisotropic media are provided in Section 2. Note that, for the ray approximation to be valid, the parameters characterizing the media must be smoothly varying (Červený, 2001), *i.e.*, they do not vary significantly over a wavelength (or the Fresnel zone width). In order to compute the reflected/transmitted wave characteristics, the ray propagator matrix (from which the geometrical spreading factor is obtained) and the Fresnel matrix (which accounts for the interface curvature) are needed. They are determined in Section 3 for both heterogeneous and homogeneous anisotropic media. Section 4 presents expressions for wave amplitude and phase response in anisotropic media with a curved interface. Attention is paid to the relative geometrical spreading and to the number of caustics (KMAH index) encountered along the

ray, connecting the source and the receiver after reflection on the curved interface, since it may strongly affect the characteristics of the recorded signal by means of a sum of phase shifts. The effect of the interface is thus clearly identified in the expressions for the asymptotic Green function of the reflected and transmitted waves. Section 5 deals with the special case of homogeneous dip-constrained transversely isotropic media, for which the symmetry axis is parallel to the interface normal at each point of the interface. In order to gain insight more specifically in the focusing effect of the interface, the special case of homogeneous isotropic media separated by a curved interface is discussed in Section 6 and compared to the case of a plane interface. Section 7 provides illustrations of the impact of the curvature of an interface between dip-constrained transversely isotropic media on the amplitude and phase of the reflected P wave, with the source and the receiver on the vertical axis of the interface (the case where the source and receiver are at the same position having been treated and discussed by Bleistein (1984)). Considering a vertical seismic profile makes the P-P reflection issue in dip-constrained transversely isotropic media equivalent to the isotropic case. This particular case, although much simplified compared to the real ones dealt with in seismic exploration, is valuable for providing clear physical insight into the impact of the interface curvature only. The cases of syncline-type interfaces with a locally spherical or ellipsoidal shape are considered. Deeks & Lumley (2015) have discussed the reflection response from a seafloor canyon and have shown that, in addition to the direct reflected wave, there may be a prismatic reflection, bouncing back from two sides of the canyon. However, this only occurs if the curvature of the canyon walls have inflection points. This is not the case in our examples. 3D numerical simulations of wave reflection from the curved interfaces using a spectral-element method (*e.g.*, (Komatitsch & Vilotte, 1998; Fichtner, 2010; Peter et al., 2011)) allow to validate our analytical derivations. In particular, comparison between the numerical and the analytical results confirms the fact that using plane-wave reflection coefficient without correction for the interface effect may lead to wrong interpretation of AVA/AVO analysis.

In the work presented here we do not take explicitly the effect of the interface Fresnel zone (Favretto-Cristini et al., 2009; Ursin et al., 2014) into account in our analytical derivations, despite its significant impact on amplitude of the reflected and transmitted waves (Favretto-Cristini et al., 2007a), in particular when the incident wavefront curvature tends to the reflector curvature (possible existence of bright spots), and its impact on estimation of media properties (Favretto-Cristini et al., 2007b). We assume that in the high-frequency approximation this impact is small, in particular for the case of vertical seismic profiles (as considered in the illustrative part of this paper). However, for horizontal seismic profiles the interface Fresnel

zone might be implicitly accounted for in the formulation of the reflection coefficients under the form of effective reflection coefficients, as effective reflection coefficients account for the frequency spectrum of the incident wavefield. It allows to correctly reproduce for instance the near- and supercritical effects, in particular the slowness interferences of reflected and head waves within the interface Fresnel zone (Favretto-Cristini et al., 2007a; Ayzenberg et al., 2007; Skopintseva et al., 2012).

2 RAY TRACING IN ANISOTROPIC MEDIA

We consider a ray for a reflected or transmitted wave at a point on a curved interface. At this point the $x_1 - x_2$ plane is tangent to the interface. The curved interface Σ which separates the two media can locally be approximated by a second-order expression

$$x_3 = (x_1\,,\, x_2)\ \mathbf{D}\ (x_1\,,\, x_2)^T = D_{11}\, x_1^2 + (D_{12} + D_{21})\ x_1\, x_2 + D_{22}\, x_2^2, \tag{1}$$

where $\mathbf{D}$ is the 2 x 2 curvature matrix and the superscript ^{T} denotes the transpose of a quantity.

The horizontal slowness of the incoming ray is along the x_1-axis. Then the slownesses of the incoming and the outgoing waves are :

$$\mathbf{p} = (p_1,\, 0,\, p_3)^T = \left(\frac{\sin\theta}{c},\, 0,\, \frac{\cos\theta}{c}\right)^T \tag{2}$$

$$\tilde{\mathbf{p}} = (\tilde{p}_1,\, 0,\, \tilde{p}_3)^T = \left(\frac{\sin\tilde{\theta}}{\tilde{c}},\, 0,\, \frac{\cos\tilde{\theta}}{\tilde{c}}\right)^T, \tag{3}$$

respectively. Here, c (respectively, $\tilde{c}$) is the phase velocity of the medium of the incident (respectively, reflected or transmitted) wave. Note that in the following all variables related to the incoming wave will be denoted in a standard way (like c), whereas the variables related to the outgoing (reflected or transmitted) wave will be denoted with a tilde above (like $\tilde{c}$).
Snell's law implies that the horizontal slownesses are equal :

$$p_1 = \frac{\sin\theta}{c} = \frac{\sin\tilde{\theta}}{\tilde{c}} = \tilde{p}_1 \tag{4}$$

The vertical slownesses p_3 and $\tilde{p}_3$ depend on the media parameters and the wave type. In ray tracing we may solve the Christoffel equation (*e.g.*, Chapman (2004)) :

$$(\Gamma_{ik} - G\,\delta_{ik})\ g_k = 0\,, \tag{5}$$

where

$$\Gamma_{ik} = a_{ijkl}\, p_j\, p_l \quad (i,j,k,l = 1,2,3) \tag{6}$$

is the 3 x 3 Christoffel matrix with $a_{ijkl} = {}^{c_{ijkl}}/_{\rho}$ being the real density-normalized elastic moduli, $p_j = {}^{\partial T}/_{\partial x_j}$ are the components of the 3 x 1 slowness vector $\mathbf{p}$, $T(\mathbf{x})$ being the traveltime and $\mathbf{x} = (x_1,\, x_2,\, x_3)^T$ the position vector of a point on the ray. Note that in Eq.(6) the Einstein summation rule over repeated index has been used. The Christoffel matrix is symmetric and positive definite. It has three positive eigenvalues $G(\mathbf{x},\, \mathbf{p})$ with corresponding unit vectors $\mathbf{g}(\mathbf{x},\, \mathbf{p})$ being the polarization vectors of the waves. They are the solution of the Christoffel equation (5). The eigenvalues $G(\mathbf{x},\, \mathbf{p})$ are the roots of the associated characteristic equation

$$\det\left(\Gamma_{ik} - G\,\delta_{ik}\right) = 0\,. \tag{7}$$

With the help of the Hamiltonian defined by (*e.g.*, Chapman (2004))

$$H(\mathbf{x},\, \mathbf{p}) = \frac{1}{2}\, G(\mathbf{x},\, \mathbf{p}) = \frac{1}{2}\, g_i\, \Gamma_{ik}\, g_k = \frac{1}{2}\, a_{ijkl}\, p_j\, p_l\, g_i\, g_k = \frac{1}{2}\,, \tag{8}$$

we can get the kinematic ray-tracing equations, namely the components of the ray (or group) velocity vector $\mathbf{V} = (V_1,\, V_2,\, V_3)^T$:

$$\frac{d\,x_j}{d\,\tau} = V_j = \frac{\partial\, H}{\partial\, p_j} = \frac{1}{2}\, a_{ijkl}\, p_l\, g_i\, g_k \tag{9}$$

and the components of the so-called eta vector $\boldsymbol{\eta} = (\eta_1,\, \eta_2,\, \eta_3)^T$ which describes the rate of change in the slowness direction :

$$\frac{d\,p_n}{d\,\tau} = \eta_n = -\frac{\partial\, H}{\partial\, x_n} = -\frac{1}{2}\, \frac{\partial\, a_{ijkl}}{\partial\, x_n}\, p_j\, p_l\, g_i\, g_k\,. \tag{10}$$

Here, τ is a monotically increasing sampling parameter along the ray which represents the traveltime. We note that

$$\mathbf{p}^T\, \mathbf{V} = p_i\, \frac{\partial\, H}{\partial\, p_i} = 1 \tag{11}$$

Different methods to compute the group velocity are discussed in Zhou & Greenhalgh (2004).

3 THE FRESNEL MATRIX FOR ANISOTROPIC MEDIA

3.1 General case

In order to compute the amplitude and phase of the reflected/transmitted wave we need the Fresnel matrix (Hubral et al., 1995; Červený, 2001) which is computed from the 4 x 4 ray propagator matrix (Červený, 2001; Chapman, 2004)

$$\mathbf{\Pi} = \begin{pmatrix} \mathbf{Q_1} & \mathbf{Q_2} \\ \mathbf{P_1} & \mathbf{P_2} \end{pmatrix} \tag{12}$$

For the reflected/transmitted ray the total ray propagator matrix is

$$\overline{\mathbf{\Pi}} = \widetilde{\mathbf{\Pi}}\, \widetilde{\mathbf{Y}}^{-1}\, \mathbf{Y}\, \mathbf{\Pi} \tag{13}$$

where $\mathbf{\Pi}$ is the ray propagator from the source to the interface point and $\widetilde{\mathbf{\Pi}}$ the ray propagator from the interface point to the receiver. The interface ray propagator transformation matrix for the incoming ray is

$$\mathbf{Y} = \begin{bmatrix} \mathbf{K^{-T}} & \mathbf{0} \\ \mathbf{W\, K^{-T}} & \mathbf{K} \end{bmatrix} \tag{14}$$

where (see Appendix A)

$$\mathbf{K} = \begin{bmatrix} \frac{V_3}{c} & -p_1\, V_2 \\ 0 & 1 \end{bmatrix} \tag{15}$$

$$\mathbf{K^{-T}} = \begin{bmatrix} \frac{c}{V_3} & 0 \\ c\, p_1\, \frac{V_2}{V_3} & 1 \end{bmatrix} \tag{16}$$

and

$$\mathbf{W} = \mathbf{E} + p_3\, \mathbf{D}\,. \tag{17}$$

Here, $\mathbf{D}$ is the curvature matrix of the interface and $\mathbf{E}$ is the inhomogeneity matrix given by

$$\mathbf{E} = \begin{bmatrix} E_{11} & 0 \\ 0 & 0 \end{bmatrix} \tag{18}$$

with

$$E_{11} = p_1\, \eta_1 + p_1\, V_3\, (p_3\, \eta_1 - p_1\, \eta_3) \tag{19}$$

Note that $\eta_2 = 0$. For the outgoing ray the interface ray propagator transformation matrix can be written as

$$\widetilde{\mathbf{Y}}^{-1} = \begin{bmatrix} \widetilde{\mathbf{K}}^{\mathbf{T}} & \mathbf{0} \\ -\widetilde{\mathbf{K}}^{-1}\widetilde{\mathbf{W}} & \widetilde{\mathbf{K}}^{-1} \end{bmatrix} \tag{20}$$

Here, $\widetilde{\mathbf{W}}$ and $\widetilde{\mathbf{K}}$ are defined in a similar way as $\mathbf{W}$ and $\mathbf{K}$.

From Eq.(13) we obtain (Červený, 2001)

$$\overline{\mathbf{Q}}_{\mathbf{2}} = \widetilde{\mathbf{Q}}_{\mathbf{1}}\,\widetilde{\mathbf{K}}^{T}\,\mathbf{K}^{-T}\,\mathbf{Q}_{\mathbf{2}} + \widetilde{\mathbf{Q}}_{2}\,\widetilde{\mathbf{K}}^{-1}\,\Delta\mathbf{W}\,\mathbf{K}^{-T}\,\mathbf{Q}_{\mathbf{2}} + \widetilde{\mathbf{Q}}_{2}\,\widetilde{\mathbf{K}}^{-1}\,\mathbf{K}\,\mathbf{P}_{\mathbf{2}} \tag{21}$$

where $\Delta\mathbf{W} = \mathbf{W} - \widetilde{\mathbf{W}}$. That is

$$\overline{\mathbf{Q}}_{\mathbf{2}} = \widetilde{\mathbf{Q}}_{2}\,\mathbf{F}\,\mathbf{Q}_{\mathbf{2}} \tag{22}$$

where the Fresnel matrix $\mathbf{F}$ is

$$\mathbf{F} = \widetilde{\mathbf{Q}}_{\mathbf{2}}^{-1}\,\widetilde{\mathbf{Q}}_{\mathbf{1}}\,\widetilde{\mathbf{K}}^{T}\,\mathbf{K}^{-T} + \widetilde{\mathbf{K}}^{-1}\,\Delta\mathbf{W}\,\mathbf{K}^{-T} + \widetilde{\mathbf{K}}^{-1}\,\mathbf{K}\,\mathbf{P}_{\mathbf{2}}\,\mathbf{Q}_{\mathbf{2}}^{-1} \tag{23}$$

3.2 Case of homogeneous media

We now consider two homogeneous anisotropic media separated by a curved interface and an incoming wave which is reflected or transmitted at a point O at this interface, as shown in Figure 1. We define an orthogonal coordinate system at O, with the x_3-axis pointing along the interface normal into the medium of transmitted waves, and the x_2-axis normal to the plane defined by the slowness of the incoming wave and the interface normal. We denote this 3D local Cartesian system as the reflector coordinate system. We consider that the source is located at $\mathbf{x^s} = (x_1^s,\, x_2^s,\, x_3^s)$ at a distance

$$d = \|\mathbf{x^s}\| = \left[(x_1^s)^2 + (x_2^s)^2 + (x_3^s)^2\right]^{\frac{1}{2}} \tag{24}$$

from the reflection/transmission point O, the vector $\mathbf{x^s}$ being the source position vector. The receiver point can be located either in the incident medium, or in the transmitted medium, at $\tilde{\mathbf{x}} = (\tilde{x}_1,\, \tilde{x}_2,\, \tilde{x}_3)$ at a distance $\tilde{d}$ from the reflection/transmission point O. For the source we then have :

$$x_3^s = -\frac{d}{V}\,V_3 \tag{25}$$

and for the receiver :

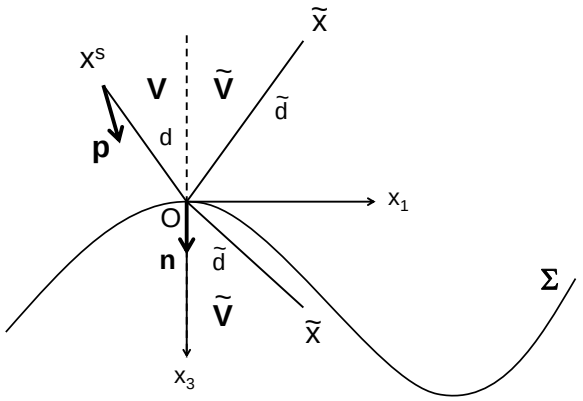

Figure 1. Incident, reflected and transmitted waves at a curved interface Σ between two homogeneous anisotropic media

$$\tilde{x}_3 = \frac{\tilde{d}}{\widetilde{V}}\,\widetilde{V}_3\ , \tag{26}$$

where V_3 (respectively, $\widetilde{V}_3$) is the component, along the x_3-axis, of the group velocity vector $\mathbf{V}$ (respectively, $\widetilde{\mathbf{V}}$). It points downwards for the incident and transmitted waves, and hence has a positive value, whereas it points upwards for the reflected wave (hence, $\widetilde{V}_3 < 0$). Eqs(25) and (26) give the ray distances d and $\tilde{d}$, respectively.

Since the media are homogeneous, the propagator matrix $\mathbf{\Pi}$ for the wave coming from the source at $\mathbf{x^s}$ can be expressed as

$$\mathbf{\Pi}\,(\mathbf{x},\ \mathbf{x^s}) = \begin{pmatrix} \mathbf{I} & \mathbf{Q_2} \\ \mathbf{0} & \mathbf{I} \end{pmatrix} \tag{27}$$

with

$$\mathbf{Q_2} = \frac{d}{V}\,\frac{\partial^2 H}{\partial p\,\partial p^T}\ . \tag{28}$$

The propagator matrix $\widetilde{\mathbf{\Pi}}$ for the outgoing wave is similarly defined with appropriate $\widetilde{\mathbf{Q}}_\mathbf{2}$. Moreover, for homogeneous media the inhomogeneity matrix $\mathbf{E}$ reduces to zero, and then

$$\Delta\mathbf{W} = (p_3 - \tilde{p}_3)\ \mathbf{D} = \Delta p_3\ \mathbf{D} \tag{29}$$

The Fresnel matrix $\mathbf{F}$ in Eq.(23) then simplifies to

$$\mathbf{F} = \widetilde{\mathbf{Q}}_\mathbf{2}^{-1}\,\widetilde{\mathbf{K}}^T\,\mathbf{K}^{-T} + \widetilde{\mathbf{K}}^{-1}\,\Delta p_3\,\mathbf{D}\,\mathbf{K}^{-T} + \widetilde{\mathbf{K}}^{-1}\,\mathbf{K}\,\mathbf{Q}_\mathbf{2}^{-1} \tag{30}$$

since $\widetilde{\mathbf{Q}}_\mathbf{1} = \mathbf{P}_\mathbf{2} = \mathbf{I}$.

4 WAVE AMPLITUDE AND PHASE RESPONSE IN ANISOTROPIC MEDIA

We want to compute the amplitude and phase response of a wave traveling from the source at $\mathbf{x^s}$, reflected or transmitted and possibly mode-converted at O, and then traveling further to $\tilde{\mathbf{x}}$. We shall use the geometrical ray approximation for the Green function. The Green function for a specific wave type from $\mathbf{x^s}$ to $\mathbf{x}$ is then given by (Červený, 2001; Chapman, 2004)

$$G_{jk}\left(\mathbf{x},\,\mathbf{x^s}\right) = \frac{\exp\left[i\,\omega\,T\left(\mathbf{x},\,\mathbf{x^s}\right)\right]\,\exp\left[-i\frac{\pi}{2}\,\mathrm{sgn}\left(\omega\right)\,\kappa\left(\mathbf{x},\,\mathbf{x^s}\right)\right]\,g_j\left(\mathbf{x}\right)\,g_k\left(\mathbf{x^s}\right)}{4\pi\,\left[\rho\left(\mathbf{x}\right)\,c\left(\mathbf{x}\right)\,\rho\left(\mathbf{x^s}\right)\,c\left(\mathbf{x^s}\right)\,\left|\det\,\mathbf{Q_2}\left(\mathbf{x},\,\mathbf{x^s}\right)\right|\right]^{1/2}}\,, \tag{31}$$

where $\omega = 2\pi f$ is the angular frequency with f the frequency, $\rho\left(\mathbf{x}\right)$ the density, $c\left(\mathbf{x}\right)$ the phase velocity, $T\left(\mathbf{x},\,\mathbf{x^s}\right)$ the traveltime from $\mathbf{x^s}$ to $\mathbf{x}$, $\kappa\left(\mathbf{x},\,\mathbf{x^s}\right)$ the KMAH index, and $\left|\det\,\mathbf{Q_2}\left(\mathbf{x},\,\mathbf{x^s}\right)\right|^{1/2}$ the relative geometrical spreading.

The asymptotic Green function for a specific reflected or transmitted, and possibly mode-converted wave between two anisotropic media is then (Červený, 2001; Schleicher et al., 2001)

$$\begin{aligned}\overline{G}_{jk}\left(\tilde{\mathbf{x}},\,\mathbf{x^s}\right) = &\frac{\widetilde{R}\left(p_1\right)\,\exp\left[i\,\omega\,\left(T\left(\mathbf{x},\,\mathbf{x^s}\right)+\widetilde{T}\left(\tilde{\mathbf{x}},\,\mathbf{x}\right)\right)\right]}{\times\,\exp\left[-i\frac{\pi}{2}\,\mathrm{sgn}\left(\omega\right)\,\left(\kappa\left(\mathbf{x},\,\mathbf{x^s}\right)+\tilde{\kappa}\left(\tilde{\mathbf{x}},\,\mathbf{x}\right)+\kappa^F\right)\right]\,g_j\left(\tilde{\mathbf{x}}\right)\,g_k\left(\mathbf{x^s}\right)}\\ &4\pi\,\left[\rho\left(\tilde{\mathbf{x}}\right)\,c\left(\tilde{\mathbf{x}}\right)\,\rho\left(\mathbf{x^s}\right)\,c\left(\mathbf{x^s}\right)\,\left|\det\,\overline{\mathbf{Q}}_\mathbf{2}\left(\tilde{\mathbf{x}},\,\mathbf{x^s}\right)\right|\right]^{1/2}\end{aligned} \tag{32}$$

Here, $\widetilde{R}\left(p_1\right)$ is the reflection or transmission coefficient at the interface, normalized with respect to vertical energy flux, as indicated in (Chapman, 1994; Schleicher et al., 2001). The relative geometrical spreading $\left|\det\,\overline{\mathbf{Q}}_\mathbf{2}\left(\tilde{\mathbf{x}},\,\mathbf{x^s}\right)\right|^{1/2}$ between $\mathbf{x^s}$ and $\tilde{\mathbf{x}}$ depends on the relative geometrical spreading between $\mathbf{x^s}$ and a point $\mathbf{x}$ on the interface, and the relative geometrical spreading between $\mathbf{x}$ and $\tilde{\mathbf{x}}$, through (see Eq.(22))

$$\left|\det\,\overline{\mathbf{Q}}_\mathbf{2}\left(\tilde{\mathbf{x}},\,\mathbf{x^s}\right)\right|^{1/2} = \left[\left|\det\,\widetilde{\mathbf{Q}}_\mathbf{2}\left(\tilde{\mathbf{x}},\,\mathbf{x}\right)\right|\,\left|\det\,\mathbf{F}\right|\,\left|\det\,\mathbf{Q_2}\left(\mathbf{x},\,\mathbf{x^s}\right)\right|\right]^{1/2}\,. \tag{33}$$

The change in the KMAH index is the KMAH index for the Fresnel matrix $\mathbf{F}$

$$\kappa^F = 1 - \frac{1}{2}\,\mathrm{sgn}\left(\mathbf{F}\right), \tag{34}$$

$\mathrm{sgn}\left(\mathbf{F}\right)$ being the difference between the number of its positive and negative eigenvalues.

The effect of the interface on the asymptotic Green function of the reflected or transmitted wave is characterized more specifically by the factor

$$A = \frac{\exp\left[-i\frac{\pi}{2}\,\mathrm{sgn}\,(\omega)\;\kappa^F\right]}{|\det\,\mathbf{F}|^{1/2}}\,. \tag{35}$$

Using

$$\overline{R}\,(p_1) = \widetilde{R}\,(p_1)\;\frac{\exp\left[-i\frac{\pi}{2}\,\mathrm{sgn}\,(\omega)\;\kappa^F\right]}{|\det\,\mathbf{F}|^{1/2}} \tag{36}$$

without correction for the effect of the Fresnel matrix $\mathbf{F}$ (*i.e.* without removing the factor A) may thus lead to wrong interpretation of an AVA analysis. For instance, for a reflected wave, amplitude variations with incidence angle may be due to changes in the reflection coefficient and changes in the relative geometrical spreading, related to the Fresnel matrix. Phase changes may be due to a polarity reversal in the reflection coefficient. There may also be a phase shift due to the curved interface, determined by the Fresnel matrix. In Eqs (32) and(36) we normally consider the exact or linearized plane-wave reflection coefficient, since this reflection coefficient is still currently the most used in AVO/AVA inversion. However, as already mentioned in the Introduction, in the near field or for large offsets near the critical angle we may replace it with the spherical-wave reflection coefficient or with the effective reflection coefficient.

5 SPECIAL CASE OF HOMOGENEOUS DIP-CONSTRAINED TRANSVERSELY ISOTROPIC MEDIA

To provide analytic insight into the influence of anisotropy, we apply the previous theory to the case of a curved interface between two dip-constrained transversely isotropic media. Since the symmetry axis of both media is parallel to the interface normal at each point of the interface, at the reflection point, both halfspaces are VTI in the local reflector coordinate system. The three wave types which may occur are then the SH wave and coupled P-SV waves. Because of the symmetry, all seismic signatures depend only on the angle between the propagation direction and the symmetry axis. The out-of-plane components of the group velocity vector and slowness vector are equal to zero in all cases ($V_2 = p_2 = 0$), and x_2 is equal to zero as well.

From Eqs(15) and(16) we then get

$$\mathbf{K} = \mathbf{K}^T = \begin{bmatrix} \frac{V_3}{c} & 0 \\ 0 & 1 \end{bmatrix} \tag{37}$$

$$\mathbf{K}^{-1} = \mathbf{K}^{-T} = \begin{bmatrix} \frac{c}{V_3} & 0 \\ 0 & 1 \end{bmatrix} \tag{38}$$

The group velocity components are given in Appendix B, and

$$V_3 = \frac{1}{p_3 - p_1\, p_3^{'}} \tag{39}$$

where the derivative is

$$p_3^{'} = \frac{d\, p_3}{d\, p_1} \tag{40}$$

The phase velocity can be computed from Ursin & Stovas (2006)

$$\frac{1}{c^2} = p_1^2 + p_3^2 = \frac{1}{2}\left[\frac{1}{\alpha_0^2} + \frac{1}{\beta_0^2} + \zeta\, p_1^2 \mp \left(\sigma_0^2 + \xi\, p_1^2 + \chi\, p_1^4\right)^{1/2}\right] \tag{41}$$

with $-$ for a P wave and $+$ for a SV wave. Here, α_0 and β_0 are the vertical P- and SV-wave velocities, respectively, and $\sigma_0 = \frac{1}{\alpha_0^2} - \frac{1}{\beta_0^2}$. The constants are

$$\begin{cases} \zeta = -2\ (\delta + \sigma) \\ \xi = -4\, \sigma_0\ (\delta - \sigma) \\ \chi = 4\ \left[-2\, \beta_0^2\, \sigma_0\, \sigma + (\sigma + \delta)^2\right] \end{cases} \tag{42}$$

where we have used (Thomsen, 1986) parameters

$$\begin{cases} \sigma = \frac{c_{33}}{c_{44}}\ (\epsilon - \delta) \\ \epsilon = \frac{c_{11} - c_{33}}{2\, c_{33}} \\ \delta = \frac{(c_{13} + c_{44})^2 - (c_{33} - c_{44})^2}{2\, c_{33}\, (c_{33} - c_{44})} \end{cases} \tag{43}$$

Expanding the square root in Eq.(41) in a Taylor series and neglecting a square term in the anisotropy parameters result in very simple expressions

$$\frac{1}{c^2} \simeq \begin{cases} \frac{1}{\alpha_0^2} - 2\, \delta\, p_1^2 - 2\, \beta_0^2\, \sigma\, p_1^4 & (P\ wave) \\ \frac{1}{\beta_0^2} - 2\, \sigma\, p_1^2 + 2\, \beta_0^2\, \sigma\, p_1^4 & (SV\ wave) \end{cases} \tag{44}$$

Furthermore, the inverse of the relative geometrical spreading matrix is (see Appendix C)

$$\mathbf{Q_2}^{-1} = -\frac{1}{x_3} \begin{bmatrix} \frac{1}{\cos^2 \alpha\, p_3^{''}} & 0 \\ 0 & \frac{p_1}{p_3^{'}} \end{bmatrix} = \begin{bmatrix} g_{11} & 0 \\ 0 & g_{22} \end{bmatrix} \tag{45}$$

where α is the ray angle. With these simplifications, the Fresnel matrix in Eq.(30) has components

$$\begin{cases} F_{11} = \frac{\tilde{V}_3}{\tilde{c}}\ \frac{c}{V_3}\ \tilde{g_{11}} + \frac{\tilde{c}}{\tilde{V}_3}\ \frac{V_3}{c}\ g_{11} + (p_3 - \tilde{p}_3)\ D_{11}\ \frac{c}{V_3}\ \frac{\tilde{c}}{\tilde{V}_3} \\ F_{22} = \tilde{g_{22}} + g_{22} + (p_3 - \tilde{p}_3)\ D_{22} \\ F_{12} = \frac{\tilde{c}}{\tilde{V}}\ (p_3 - \tilde{p}_3)\ D_{12} \\ F_{21} = \frac{c}{V_3}\ (p_3 - \tilde{p}_3)\ D_{21} \end{cases} \tag{46}$$

where g_{kk} and $\tilde{g_{kk}}$ are as defined in Eq.(45) above for the incoming and outgoing wave, respectively.

6 SPECIAL CASE OF HOMOGENEOUS ISOTROPIC MEDIA

The results in the previous sections are valid for reflected or transmitted, possibly mode-converted waves in anisotropic media. In order to gain insight more specifically in the focusing effect of the interface we shall consider here the particular case of two homogeneous isotropic media separated by a curved reflector. In this case, the group and phase velocities are the same (related to the P or S waves, respectively).

The propagator matrix $\mathbf{\Pi}$ for the wave coming from the source at $\mathbf{x^s}$ to the reflection/transmission point at $\mathbf{x}$ is of the form (27) with $\mathbf{Q_2} = c\,d\,\mathbf{I}$, where $d = \left[(x_1^s)^2 + (x_3^s)^2\right]^{\frac{1}{2}}$ is the distance from the source to the point O, since $x_2^s = 0$. The propagator matrix $\widetilde{\mathbf{\Pi}}$ for the outgoing wave is similarly defined. Since $\frac{V_3}{c} = \cos\theta$, we have

$$\mathbf{K} = \begin{bmatrix} \cos\theta & 0 \\ 0 & 1 \end{bmatrix}, \tag{47}$$

and the Fresnel matrix in Eq.(30) can now be expressed as

$$\mathbf{F} = \frac{1}{\tilde{c}\,\tilde{d}} \begin{bmatrix} \frac{\cos\tilde{\theta}}{\cos\theta} & 0 \\ 0 & 1 \end{bmatrix} + \frac{1}{c\,d} \begin{bmatrix} \frac{\cos\theta}{\cos\tilde{\theta}} & 0 \\ 0 & 1 \end{bmatrix} + \Delta p_3 \begin{bmatrix} \frac{1}{\cos\tilde{\theta}} & 0 \\ 0 & 1 \end{bmatrix} \mathbf{D} \begin{bmatrix} \frac{1}{\cos\theta} & 0 \\ 0 & 1 \end{bmatrix}. \tag{48}$$

where $\Delta p_3 = p_3 - \tilde{p}_3$.

For a non-converted (*i.e.*, P-P or S-S) reflected wave, we have $c = \tilde{c}$, $\theta = \tilde{\theta}$, $p_3 = \frac{\cos\theta}{c}$ and $\tilde{p}_3 = -\frac{\cos\theta}{c}$. This gives

$$\Delta p_3 = 2\,\frac{\cos\theta}{c} \tag{49}$$

and the Fresnel matrix in Eq.(48) is now written as :

$$\mathbf{F} = \frac{1}{c} \left\{ \left(\frac{1}{\tilde{d}} + \frac{1}{d} \right) \mathbf{I} + 2 \begin{bmatrix} 1 & 0 \\ 0 & \cos\theta \end{bmatrix} \mathbf{D} \begin{bmatrix} \frac{1}{\cos\theta} & 0 \\ 0 & 1 \end{bmatrix} \right\} , \tag{50}$$

or

$$\mathbf{F} = \frac{1}{c} \left\{ \left(\frac{1}{\tilde{d}} + \frac{1}{d} \right) \mathbf{I} + 2 \begin{bmatrix} \frac{D_{11}}{\cos\theta} & D_{12} \\ D_{21} & D_{22}\cos\theta \end{bmatrix} \right\} . \tag{51}$$

For a vertical seismic profile with the source and receivers straight above the reflector (but not necessarily overlapped), we have $\cos\theta = \cos\tilde{\theta} = 1$. If the axes of the coordinate system coincide with the main axes of the interface curvature matrix, so that $D_{12} = D_{21} = 0$ and $D_{11} = \frac{\mu_1}{R_1}$ and $D_{22} = \frac{\mu_2}{R_2}$, where $\mu_{1,2} = -1$ (respectively, $\mu_{1,2} = +1$) for a syncline-type reflector (respectively, an anticline-type reflector) and $R_{1,2}$ is the curvature radius of the interface, Eq.(51) then becomes

$$\mathbf{F} = \frac{1}{c} \left\{ \left(\frac{1}{\tilde{d}} + \frac{1}{d} \right) \mathbf{I} + 2 \begin{bmatrix} \frac{\mu_1}{R_1} & 0 \\ 0 & \frac{\mu_2}{R_2} \end{bmatrix} \right\} \tag{52}$$

and

$$|\det \mathbf{F}|^{1/2} = \frac{1}{c} \left| \left(\frac{1}{\tilde{d}} + \frac{1}{d} + 2\,\frac{\mu_1}{R_1} \right) \left(\frac{1}{\tilde{d}} + \frac{1}{d} + 2\,\frac{\mu_2}{R_2} \right) \right|^{1/2} . \tag{53}$$

For a plane reflector, Eq.(53) reduces to

$$|\det \mathbf{F}|^{1/2} = \frac{1}{c} \left(\frac{1}{\tilde{d}} + \frac{1}{d} \right) . \tag{54}$$

From Eqs.(35), (36), (53) and (54), we can see that, in order to correct for the effect of the reflector curvature, the data amplitude should be multiplied by

$$C = \frac{A_{plane}}{A_{curved}} = \frac{\left| \left(\frac{1}{\tilde{d}} + \frac{1}{d} + 2\,\frac{\mu_1}{R_1} \right) \left(\frac{1}{\tilde{d}} + \frac{1}{d} + 2\,\frac{\mu_2}{R_2} \right) \right|^{1/2}}{\left(\frac{1}{\tilde{d}} + \frac{1}{d} \right)} \exp\left[+i\frac{\pi}{2} \operatorname{sgn}(\omega)\, \kappa^F \right] , \tag{55}$$

where

$$\kappa^F = 1 - \frac{1}{2} \left[\operatorname{sgn}\left(\frac{1}{\tilde{d}} + \frac{1}{d} + 2\,\frac{\mu_1}{R_1} \right) + \operatorname{sgn}\left(\frac{1}{\tilde{d}} + \frac{1}{d} + 2\,\frac{\mu_2}{R_2} \right) \right] . \tag{56}$$

Expression (55) is valid only for a reflected P-P or S-S wave with the source and the receiver on the vertical axis of the interface between two isotropic media. A slightly more complicated expression can be obtained for a transmitted wave with similar geometry. Note that the case

where the source and receiver are at the same position has been treated and discussed by Bleistein (1984) (see there Eq. (8.4.32)).

Let us consider a syncline-type reflector ($\mu_{1,2} = -1$) with $R_1 < R_2$ and a fixed position d of the source relative to the reflection point at the interface. From Eq. (56) we can derive the critical position(s) $\tilde{d}$ of the receiver relative to the reflector for which a phase change occurs :

(i) for $\frac{1}{\tilde{d}} + \frac{1}{d} > \frac{2}{R_1}$, or more explicitly for $\tilde{d} < \left(\frac{2}{R_1} - \frac{1}{d}\right)^{-1} < R_1$, there is no phase change as $\kappa^F = 0$,

(ii) for $\frac{2}{R_2} < \frac{1}{\tilde{d}} + \frac{1}{d} < \frac{2}{R_1}$, or more explicitly for $\left(\frac{2}{R_1} - \frac{1}{d}\right)^{-1} < \tilde{d} < \left(\frac{2}{R_2} - \frac{1}{d}\right)^{-1} < R_2$, there is a phase change of $\frac{\pi}{2}$ as $\kappa^F = 1$,

(iii) for $\frac{1}{\tilde{d}} + \frac{1}{d} < \frac{2}{R_2}$, or more explicitly for $\tilde{d} > \left(\frac{2}{R_2} - \frac{1}{d}\right)^{-1}$, there is a polarity reversal as $\kappa^F = 2$.

7 NUMERICAL ILLUSTRATIONS

Our purpose here is to gain insight into the impact of the interface curvature on the wave amplitude and phase response. To illustrate this impact, we do not consider transmitted waves and focus only on the wave reflection at a curved interface. We are more particularly interested in P-P reflection from interfaces of syncline type, since this kind of interfaces may generate caustics. We focus more specifically on two cases :1) an interface with $R_1 = R_2$, and 2) an interface with $R_1 \neq R_2$. For the first case, two different shapes of interface are considered, namely a truncated spherical shape (Figure 2, left side) and a truncated ellipsoid shape (Figure 2, right side). For the second case, the interface shape is a truncated ellipsoid of revolution that combines the two shapes illustrated in Figure 2.

To illustrate our purpose, we consider dip-constrained transversely isotropic media for which the symmetry axis is parallel to the interface normal at each point of the interface. At the reflection point, media are VTI in the local coordinate system because the symmetry axis is parallel to the x_3-axis. Because of the symmetry, all seismic signatures then depend only on the angle between the propagation direction and the symmetry axis. In addition, we consider a seismic vertical profile for which the source and the array of receivers are on the same vertical line colinear to the x_3-axis at the reflection point. As a consequence, the P-P reflection issue in dip-constrained transversely isotropic media is equivalent to the isotropic case. This particular case, although much simplified compared to the real ones dealt with in seismic exploration, is valuable for providing clear physical insight into the impact of the interface curvature only.

Hereafter, the source is located at a distance of 800 m from the interface at the reflection

Figure 2. Configurations considered in the 3D numerical simulations of wave reflection from curved interfaces : (left side) interface of truncated spherical shape, (right side) interface of truncated ellipsoid shape. S denotes the source location, whereas R denotes the receiver array location.

point. An array of receivers is distributed along the axis that connects the source to the reflection point; the receivers are located every $100\,m$ from a distance of $100\,m$ up to a distance of $900\,m$ from the interface. This configuration enables to limit as much as possible the diffraction effects by the edges of the interfaces of finite size. We consider that the incidence medium has the density $\rho_1 = 1\,000\,kg/m^3$ and the P-wave velocity $V_{P1} = 1\,500\,m/s$, whereas the transmission medium has the density $\rho_2 = 1\,800\,kg/m^3$ and the P-wave velocity $V_{P2} = 1\,900\,m/s$.

In order to validate our analytical derivations, we have conducted 3D numerical simulations of wave reflection from the curved interfaces using a spectral-element method (*e.g.*, Komatitsch & Vilotte (1998), Fichtner (2010), Peter et al. (2011)). Specifically, we used the SPECFEM software package (https://geodynamics.org/cig/software/specfem3d/). The spectral-element method is based upon a high-order piecewise polynomial approximation of the weak formulation of the wave equation and combines the accuracy of the pseudospectral method with the flexibility of the finite-element method. In this method, the wavefield is represented in terms of high-degree Lagrange interpolants, and integrals are computed based upon Gauss–Lobatto–Legendre quadrature, thus leading to a perfectly diagonal mass matrix, and in turn to a fully explicit time scheme that lends itself very well to numerical simulations on parallel computers (*e.g.*, Carrington et al. (2008)). We have relied on a time scheme that is classically used with the spectral-element method, namely a second-order Newmark scheme. The meshing of the 3D computational domain has been made with Cubit/Trelis software (Blacker (1994)). The main difficulty in obtaining a reliable hexaedral mesh is related to the curvature of the interface that leads to the generation of unnecessary small elements. The size of these small elements has a strong impact on the time scheme since they require small time steps, thus increasing dramatically the total number of time steps useful to numerically model the time duration of the desired signals. In order to overcome this difficulty, we have chosen to start with a much coarser mesh, and then refine it by splitting several times. This strategy leads to a reliable mesh that has been used to perform the numerical simulations. This mesh was composed of 4 million elements. A three-element PML layer was added all around the domain in order to remove spurious reflections from the boundaries (Xie et al. (2016)). The source signal is a

Ricker wavelet with a central frequency f of 20 Hz. Typical 3D numerical simulations have lasted 1h30 on a 192-cores cluster.

7.1 Case of an interface with $R_1 = R_2$

Let us first examine the case of an interface of truncated-sphere shape with a radius of curvature of 500 m. Remembering that the source is located at a fixed position (namely, 800 m from the reflection point at the interface), the critical distance $\tilde{d}$ between the reflection point and the receiver, for which a phase shift is expected, can be easily evaluated from our analytical derivations as being equal to 363.6 m.

In order to provide physical insights in the wave propagation, Figure 3 shows snapshots at different propagation times. It has to be pointed out here that the finite size of the reflector generates two diffracted wavefronts at the edges of the curved interface that subsequently interact with the reflected wavefront. These diffractions are not accounted for in our analytical derivations. However, for a short range of receiver positions the reflected and diffracted events can be hardly separated, as it is illustrated in the numerical seismograms obtained at the receiver array (Figure 4). Nevertheless, for a wide range of receiver locations, the wavefronts are well separated, which allows to clearly highlight the phase shift of the reflected signal for receiver locations beyond the critical distance $\tilde{d} = 363.6\, m$. Note the higher amplitudes of the reflected event in the vicinity of the critical distance $\tilde{d}$. The good agreement between our analytical predictions and the numerical results is more clearly illustrated in Figure 5. Figure 5 shows the variation of the factor C, that should be applied to data amplitude to correct for the effect of the reflector curvature, as a function of the distance of the receiver from the reflection point at the interface. We can see a perfect fit between the values calculated analytically from Eq. 55 and the values obtained numerically with the help of simulations conducted for the curved interface of interest here and for a plane interface.

Let us then examine the case of an interface of a truncated-ellipsoid shape with a radius of curvature of 700 m. In this case, the critical distance $\tilde{d}$ between the reflection point and the receiver, for which a phase shift is expected, is 622.2 m. Figure 6 presents the numerical seismograms obtained at the receiver array. Higher amplitudes of the reflected event are observed when the receiver position approaches the critical distance $\tilde{d}$. A phase shift of the reflection signal is also clearly observed for receiver positions beyond the critical distance of 622.2 m.

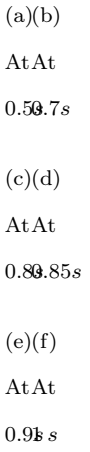

Figure 3. Snapshots of wave propagation at different times. The red star indicates the source position.

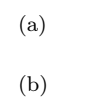

Figure 4. Numerical seismograms obtained at the receiver array, with a focus on the events reflected and diffracted by the spherically-shaped interface. The traces are normalized with respect to (a) the global maximum amplitude of all the traces, (b) the maximum amplitude of each trace. The direct arrivals have been removed from the traces. Red diamonds indicate the expected arrival times of the reflected wave. The black vertical line indicates the arrival time associated with the critical distance $\tilde{d}$ for which a phase shift of the reflected signal is expected.

Figure 5. Variation of the factor C as a function of the distance of the receiver from the reflection point at the spherically-shaped interface : comparison between the analytical predictions (Eq. 55) and the numerical results.

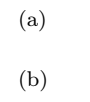

Figure 6. Numerical seismograms obtained at the receiver array, with a focus on the events reflected and diffracted by the ellipsoid-shaped interface. The traces are normalized with respect to (a) the global maximum amplitude of all the traces, (b) the maximum amplitude of each trace. The direct arrivals have been removed from the traces. Red diamonds indicate the expected arrival times of the reflected wave. The black vertical line indicates the arrival time associated with the critical distance $\tilde{d}$ for which a phase shift of the reflected signal is expected.

7.2 Case of an interface with $R_1 \neq R_2$

Let us now examine the more complex case of an interface whose shape is a truncated ellipsoid of revolution (with radii of curvature of $500\,m$ and $700\,m$, respectively), or in other terms a combination of the shapes shown in Figure 2. In this case, the critical distances $\tilde{d}$ for which phase changes are expected are then $363.6\,m$ and $622.2\,m$. Figure 7 presents the numerical seismograms obtained at the receiver array. As predicted analytically, a phase change and a polarity reversal of the reflected signal can be clearly observed. We can also note much higher amplitudes of the reflected event compared to the diffracted event.

Figure 8 shows the variation of the factor C, that should be applied to data amplitude to correct for the effect of the reflector curvature, as a function of the distance of the receiver from the reflection point at the interface. We can observe globally an excellent fit between the values calculated analytically from Eq. 55 and the values obtained numerically with the help of simulations conducted for the curved interface of interest here and for a plane interface. Misfits observed for specific ranges of the receiver position (*e.g.*, between $250\,m$ and $350\,m$, and between $600\,m$ and $700\,m$) are only due to the strong interaction between the numerical reflected and diffracted events that prevents to isolate the contribution of the reflected wave only (see Figure 7).

As the interface shape is an ellipsoid of revolution (with $R_1 = 500\,m$ and $R_2 = 700\,m$), it is interesting to compare the trend for the variation of the associated factor C with that for spherically-shaped interfaces with different curvature radius (namely, $R_1 = R_2 = 500\,m$ and $R_1 = R_2 = 700\,m$). Figure 9 shows this comparison, together with the comparison with the variation of the factor C calculated for an interface with curvature radii $R_1 = R_2 = \sqrt{500.700} \approx 592\,m$. We can see that in the vicinity of the critical distances $\tilde{d}$ (namely, $363.6\,m$ and $622.2\,m$), the values for C tend logically to those corresponding to the spherical interfaces with curvature radii of $500\,m$ and $700\,m$, respectively. However, for small and large distances of the receiver from the reflection point at the interface (*i.e.*, well below and well beyond the critical distances), the values for C tend to those corresponding to a spherical interface with curvature radii of $592\,m$.

8 CONCLUSION

Using ray theory, we have investigated analytically both the effect of the geometrical spreading and the effect of the reflector curvature on amplitude and phase changes for reflected and transmitted waves between general anisotropic media. We have also paid attention to the

(a)

(b)

Figure 7. Numerical seismograms obtained at the receiver array, with a focus on the events reflected and diffracted by the interface of ellipsoid of revolution shape. The traces are normalized with respect to (a) the global maximum amplitude of all the traces, (b) the maximum amplitude of each trace. The direct arrivals have been removed from the traces. Red diamonds indicate the expected arrival times of the reflected wave. The black vertical lines indicate the arrival times associated with the critical distances $\tilde{d}$ for which phase changes of the reflected signal are expected.

special case of homogeneous dip-constrained transversely isotropic media, for which the symmetry axis is parallel to the interface normal at each point of the interface. In order to gain insight more specifically in the focusing effect of the interface, we have discussed the special case of homogeneous isotropic media separated by a curved interface of syncline type and compared this case to the case of a plane interface. In order to validate our analytical derivations, 3D numerical modelling has been conducted using a spectral-element method for simulating wave reflection from curved interfaces of different shapes (namely, spherical, ellipsoid, and ellipsoid of revolution). Numerical seismograms obtained for a vertical seismic profile highlight that the effect of interface curvature on the reflected events is much more pronounced in a restricted area associated with the existence of caustics, which is in full agreement with our analytical predictions. Moreover, comparisons between numerical and analytical results confirm the fact that using plane-wave reflection coefficients without correction for the interface effect may lead to wrong interpretation of AVA/AVO analysis. Consequently, seismic data recorded in complex geological environments should be compensated for both geometrical spreading and interface effects before AVO/AVA analysis, in order to avoid erroneous imaging interpretation.

ACKNOWLEDGEMENTS

Bjørn Ursin thanks the Norwegian Research Council and the industry partners of the GAMES consortium for financial support (grant no. 294404). Nathalie Favretto-Cristini acknowledges

Figure 8. Variation of the factor C as a function of the distance of the receiver from the reflection point at the interface of ellipsoid of revolution shape : comparison between the analytical predictions (Eq. 55) and the numerical results.

Figure 9. Comparison of the variation of the factor C, evaluated analytically, as a function of the distance of the receiver from the reflection point at interfaces of different shapes : (blue curve) spherical shape with $R_1 = R_2 = 500\,m$, (orange curve) spherical shape with $R_1 = R_2 = 700\,m$, (red curve) ellipsoid of revolution shape with $R_1 = 500\,m$ and $R_2 = 700\,m$, (green curve) spherical shape with $R_1 = R_2 = \sqrt{500.700} \approx 592\,m$.

CNRS for financial support through the PICS BENCHIE project. This work was granted access to the High Performance Computing resources of TGCC under allocation number A0070410305 granted by GENCI. Centre de Calcul Intensif d'Aix-Marseille is also acknowledged for granting access to its high performance computing resources.

Anonymous reviewers and Editor, R.-E. Plessix, are greatly acknowledged for their careful reading of the paper and their valuable suggestions.

References

Aki, K. & Richards, P., 2002. *Quantitative seismology*, University Science Books, 2nd edn.

Alhussain, M., Gurevich, B., & Urosevic, M., 2008. Experimental verification of spherical-wave effects on the AVO response and implications for three-term inversion, *Geophysics*, **73**(2), C7–C12.

Avseth, P., Mukerji, T., & Mavko, G., 2005. *Quantitative seismic interpretation : Applying rock physics tools to reduce interpretation risk*, Cambridge University Press, Cambridge.

Ayzenberg, M., Aizenberg, A., Helle, H., Klem-Musatov, K., Pajchel, J., & Ursin, B., 2007. 3D diffraction modeling of singly scattered acoustic wavefields based on the combination of surface integral propagators and transmission operators, *Geophysics*, **72**(5), SM19–SM34.

Ayzenberg, M., Tsvankin, I., Aizenberg, A. M., & Ursin, B., 2009. Effective reflection coefficients for curved interfaces in transversely isotropic media, *Geophysics*, **74**(5), WB33–WB53.

Blacker, T., 1994. *CUBIT Mesh Generation Environment Users Manual (version october 2018)*.

Bleistein, N., 1984. *Mathematical methods for wave phenomena*, Academic Press, San Diego.

Brandsbergh-Dahl, S., de Hoop, M., & Ursin, B., 2003. Focusing in dip and AVA compensation on scattering-angle/azimuth common image gathers, *Geophysics*, **68**(1), 232–254.

Carcione, J., 2015. *Wave fields in real media*, vol. 3rd edition, Elsevier, Amsterdam.

Carrington, L., Komatitsch, D., Laurenzano, M., Tikir, M., Michéa, D., Le Goff, N., Snavely, A., & Tromp, J., 2008. High-frequency simulations of global seismic wave propagation using

SPECFEM3D_GLOBE on 62 thousand processor cores, in *SC'08: Proceedings of the 2008 ACM/IEEE conference on Supercomputing*, SC '08, pp. 60:1–60:11, IEEE Press, Austin, Texas, USA, Article #60, Gordon Bell Prize finalist ARTICLE.

Castagna, J., 1993. Petrophysical imaging using AVO, *The Leading Edge*, **12**, 172–178.

Chapman, C., 1994. Reflection/transmission coefficient reciprocities in anisotropic media, *Geophys. J. Int.*, **116**, 498–501.

Chapman, C., 2004. *Fundamentals of seismic wave propagation*, Cambridge University Press, Cambridge UK.

Deeks, J. & Lumley, D., 2015. Prism waves in seafloor canyons and their effects on seismic imaging, *Geophysics*, **80**(6), S213–S222.

Ettrich, N., Sollid, A., & Ursin, B., 2002. Out-of-plane geometrical spreading in anisotropic media, *Geophysical Prospecting*, **50**, 283–292.

Favretto-Cristini, N., Cristini, P., & de Bazelaire, E., 2007a. Influence on the Interface Fresnel zone on the reflected P-wave amplitude modelling, *Geophys. J. Int.*, **171**, 841–846.

Favretto-Cristini, N., Cristini, P., & de Bazelaire, E., 2007b. Some reflections on reflectors and wave amplitudes, *Acta Acustica united with Acustica*, **93**, 909–916.

Favretto-Cristini, N., Cristini, P., & de Bazelaire, E., 2009. What is a seismic reflector like?, *Geophysics*, **74**(1), T13–T23.

Favretto-Cristini, N., Aizenberg, A., Ursin, B., Cristini, P., & Tantsereva, A., 2017. Analysis of wave scattering from a viscoelastic layer with complex shape, *Journal of Computational Acoustics*, **25**(3), 1750023–1–1750023–12.

Fichtner, A., 2010. *Full seismic waveform modelling and inversion*, Springer-Verlag.

Gjøystdal, H., Reinharden, J., & Ursin, B., 1984. Traveltime and wavefront curvature calculation in 3D inhomogeneous layered media with curved interfaces, *Geophysics*, **49**(9), 1466–1494.

Harrison, C. & Nielsen, P., 2004. Plane-wave reflection coefficient from near-field measurements, *J. Acoust. Soc. Am.*, **116**(3), 1355–1361.

Hubral, P., 1979. A wavefront curvature approach to computing ray amplitudes in inhomogeneous media with curved interfaces, *Studia Geophysica et Geodaetica*, **23**, 131–137.

Hubral, P., Tygel, M., & Schleicher, J., 1995. Geometrical-spreading and ray-caustic decomposition of elementary seismic waves, *Geophysics*, **60**(4), 1195–1202.

Komatitsch, D. & Vilotte, J., 1998. The spectral element method: An efficient tool to simulate the seismic response of 2D and 3D geological structures, *Bulletin of the Seismological Society*

of America, **88**(2), 368–392.

Koren, Z. & Ravve, I., 2011. Full-azimuth subsurface angle domain wavefield deomposition and imaging. Part I directional and reflection image gathers, *Geophysics*, **76**(1), S1–S13.

Maultzsch, S., Horne, S., Archer, S., & Burkhardt, H., 2003. Effects of an anisotropic overburden on azimuthal amplitude analysis in horizontal transverse isotropic media, *Geophysical Prospecting*, **51**, 61–74.

Peter, D., Komatitsch, D., Luo, Y., Martin, R., Le Goff, N., Casarotti, E., Le Loher, P., Magnoni, F., Liu, Q., Blitz, C., Nissen-Meyer, T., Basini, P., & Tromp, J., 2011. Forward and adjoint simulations of seismic wave propagation on fully unstructured hexahedral meshes, *Geophys. J. Int.*, **186**(2), 721–739.

Ravve, I. & Koren, Z., 2011. Full-azimuth subsurface angle domain wavefield deomposition and imaging. Part II local angle domain, *Geophysics*, **76**(2), S51–S64.

Schleicher, J., Tygel, M., Ursin, B., & Bleistein, N., 2001. The Kirchhoff-Helmholtz integral for anisotropic elastic media, *Wave Motion*, **34**, 353–364.

Skopintseva, L., Aizenberg, A., Ayzenberg, M., Landrø, M., & Nefedkina, T., 2012. The effect of interface curvature on AVO inversion of near-critical and postcritical PP-reflections, *Geophysics*, **77**(5), N1–N16.

Stovas, A. & Ursin, B., 2003. Reflection and transmission responses of layered transversely isotropic viscoelastic media, *Geophysical Prospecting*, **51**, 447–477.

Thomsen, L., 1986. Weak elastic anisotropy, *Geophysics*, **51**(10), 1954–1966.

Ursin, B., 1986. Zero-offset reflections from a curved interface, *Geophysics*, **51**(1), 50–53.

Ursin, B. & Arntsen, B., 1985. Computation of zero-offset vertical seismic profiles including geometrical spreading and absorption, *Geophysical Prospecting*, **33**, 72–96.

Ursin, B. & Haugen, G., 1996. Weak-contrast approcimation of the elastc scattering matrix in anisotropic media, *Pure and Applied Geophysics*, **148**, 685–714.

Ursin, B. & Hokstad, K., 2003. Geometrical spreading in a layered transversely isotropic medium with vertical symmetry axis, *Geophysics*, **68**(6), 2082–2091.

Ursin, B. & Stovas, A., 2006. Traveltime approximations for a layered transversely isotropic medium, *Geophysics*, **71**(2), D23–D33.

Ursin, B. & Tjåland, E., 1996. The infrmation content of the elastic reflection matrix, *Geophys. J. Int.*, **125**, 214–228.

Ursin, B., Favretto-Cristini, N., & Cristini, P., 2014. Fresnel volume and interface Fresnel zone for reflected and transmitted waves from a curved interface in anisotropic media, *Geophysics*, **79**(5), C123–C134.

van der Baan, M. & Smit, D., 2006. Amplitude analysis of isotropic P-wave reflections, *Geophysics*, **71**(6), C93–C103.

Červený, V., 2001. *Seismic Ray Theory*, Cambridge University Press, Cambridge UK.

Červený, V. & Hron, F., 1961. Reflection coefficients for spherical waves, *Studia Geophysica et Geodaetica*, **5**, 122–132.

Červený, V. & Moser, T., 2007. Ray propagator matrices in three-dimensional anisotropic inhomogeneous layered media., *Geophys. J. Int.*, **168**, 593–604.

Červený, V., Langer, J., & Pšenčík, I., 1974. Computation of geometric spreading of seismic body waves in laterally inhomogeneous media with curved interfaces, *Geophysical Journal of the Royal Astronomical Society*, **38**(1), 9–19.

Xie, Z., Matzen, R., Cristini, P., Komatitsch, D., & Martin, R., 2016. A perfectly matched layer for fluid-solid problems: Application to ocean-acoustics simulations with solid ocean bottoms, *J. Acoust. Soc. Am.*, **140**(1), 165–175.

Xu, X. & Tsvankin, I., 2006. Anisotropic geometrical spreading correction for wide-azimuth P-wave reflections, *Geophysics*, **71**(5), D161–D170.

Xu, X., Tsvankin, I., & Pech, A., 2005. Geometrical spreading of P-wave in horizontally layered, azimuthally anisotropic media, *Geophysics*, **70**(5), D43–D53.

Yan, B., Wang, S., Ji, Y., Huang, X., & da Silva, N., 2020. Frequency-dependent spherical-wave reflection coefficient inversion in acoustic media : Theory and practice, *Geophysics*, **85**(4), R425–R435.

Zhou, B. & Greenhalgh, S., 2004. On the computation of elastic wave group velocities for a general anisotropic medium, *Journal of Geophysical Engineering*, **1**, 205–215.

Zhou, H. & McMechan, G., 2000. Analytic study of the geometrical spreading of P-wave in a layered TI medium with a vertical symmetry axis, *Geophysics*, **65**(4), 1305–1315.

Zhu, X. & McMechan, G., 2015. Amplitude and phase versus angle for elastic wide-angle reflections in the Tau-p domain, *Geophysics*, **80**(1), N1–N9.

Appendix A. The interface ray propagator transformation matrix

Several coordinate systems are needed for describing the transformation matrix for the ray propagator at an interface.

Following Červený & Moser (2007) we define a non-orthogonal interface ray-centered coordinate system

$$\mathbf{X} = [\mathbf{g_1},\, \mathbf{g_2},\, \mathbf{g_3} = \mathbf{V}] = \begin{bmatrix} 1 & 0 & V_1 \\ 0 & 1 & V_2 \\ 0 & 0 & V_3 \end{bmatrix} \tag{57}$$

where $\mathbf{g_1}$ and $\mathbf{g_2}$ are orthogonal vectors in the interface tangent plane, and $\mathbf{g_3} = \mathbf{V}$ points in the ray direction. The inverse transpose of the matrix $\mathbf{X}$ is given by

$$\mathbf{X^{-T}} = [\mathbf{h_1},\, \mathbf{h_2},\, \mathbf{h_3}] = \begin{bmatrix} 1 & 0 & 0 \\ 0 & 1 & 0 \\ -\frac{V_1}{V_3} & -\frac{V_2}{V_3} & \frac{1}{V_3} \end{bmatrix} \tag{58}$$

Furthermore, we need the non-orthogonal ray-centered coordinate system

$$\mathbf{H} = [\mathbf{e_1},\, \mathbf{e_2},\, \mathbf{e_3} = \mathbf{V}] = \begin{bmatrix} c\,p_3 & 0 & V_1 \\ 0 & 1 & V_2 \\ -c\,p_1 & 0 & V_3 \end{bmatrix} \tag{59}$$

where $\mathbf{e_1}$ and $\mathbf{e_2}$ are orthogonal vectors in the wavefront tangent plane (normal to the slowness $\mathbf{p} = (p_1,\, 0,\, p_3)^T$), and $\mathbf{e_3} = \mathbf{V}$ points in the ray direction. The inverse transpose of the matrix $\mathbf{H}$ is given by

$$\mathbf{H^{-T}} = [\mathbf{f_1},\, \mathbf{f_2},\, \mathbf{f_3} = \mathbf{p}] = \begin{bmatrix} \frac{V_3}{c} & -p_1\,V & p_1 \\ 0 & 1 & 0 \\ -\frac{V_1}{c} & -p_3\,V_2 & p_3 \end{bmatrix} \tag{60}$$

We have

$$\mathbf{f_i}^T\, \mathbf{e_k} = \delta_{\mathbf{ik}} \tag{61}$$

where Eq.(11) has been used. Note that $\mathbf{f_1}$ and $\mathbf{f_2}$ lie in the plane normal to the ray.

The ray propagator matrix is transformed as the ray is being refracted at an interface (see Červený & Moser (2007), Eqs (93) and (94)). In order to compute the transformation matrix we need the matrices (Červený & Moser (2007), Eq. (84))

$$\mathbf{K} = [\mathbf{g_1},\, \mathbf{g_2}]^T\, [\mathbf{f_1},\, \mathbf{f_2}] = \begin{bmatrix} \frac{V_3}{c} & -p_1\,V_2 \\ 0 & 1 \end{bmatrix} \tag{62}$$

and

$$\mathbf{K^{-1}} = \begin{bmatrix} \frac{c}{V_3} & c\,p_1\,\frac{V_2}{V_3} \\ 0 & 1 \end{bmatrix} \tag{63}$$

We also need the inhomogeneity matrix $\mathbf{E}$ given by Eq. (86) in Červený & Moser (2007). With our definition of the coordinate systems we obtain

$$\mathbf{E} = \begin{bmatrix} E_{11} & 0 \\ 0 & 0 \end{bmatrix} \tag{64}$$

with

$$E_{11} = p_1\,\eta_1 + p_1\,V_3\;(p_3\,\eta_1 - p_1\,\eta_3) \tag{65}$$

Note that $\eta_2 = 0$, and for a homogeneous medium we have $\mathbf{E} = \mathbf{0}$.

The transformation matrix for the incoming ray is

$$\mathbf{Y} = \begin{bmatrix} \mathbf{K^{-T}} & \mathbf{0} \\ \mathbf{W\,K^{-T}} & \mathbf{K} \end{bmatrix} \tag{66}$$

with $\mathbf{W} = \mathbf{E} + p_3\,\mathbf{D}$, where $\mathbf{D}$ is the interface curvature matrix defined in Eq.(1). For the outgoing ray we need the transformation matrix

$$\widetilde{\mathbf{Y}}^{-1} = \begin{bmatrix} \widetilde{\mathbf{K}}^{\mathbf{T}} & \mathbf{0} \\ -\widetilde{\mathbf{K}}^{-1}\widetilde{\mathbf{W}} & \widetilde{\mathbf{K}}^{-1} \end{bmatrix} \tag{67}$$

Here $\widetilde{\mathbf{W}}$ and $\widetilde{\mathbf{K}}$ are defined in a similar way as $\mathbf{W}$ and $\mathbf{K}$.

Appendix B. Group velocities in a transversely isotropic medium

We consider a ray in a homogeneous transversely isotropic medium with the symmetry axis parallel to the the x_3-axis. The horizontal distance is (see Eq. (2) and Appendix A of Ursin & Stovas (2006))

$$x_1 = x_3\,\frac{p_1 + \frac{c'}{c^3}}{p_3} = -x_3\,p_3^{'} \tag{68}$$

where the derivative q' of the variable q is with respect to the horizontal slowness p_1, and the vertical slowness is

$$p_3 = \left(\frac{1}{c^2} - p_1^2 \right)^{1/2} \tag{69}$$

The traveltime is then

$$T = \frac{x_3 \left(\frac{1}{c^2} + \frac{p_1 \, c'}{c^3} \right)}{\left(\frac{1}{c^2} - p_1^2 \right)} = x_3 \left(p_3 - p_1 \, p_3^{'} \right) \quad , \tag{70}$$

where we have used the relation $\frac{1}{c^2} = p_1^2 + p_3^2$. This gives the group velocity components

$$V_1 = \frac{x_1}{T} = \frac{-p_3^{'}}{p_3 - p_1 \, p_3^{'}} \tag{71}$$

$$V_3 = \frac{x_3}{T} = \frac{1}{p_3 - p_1 \, p_3^{'}} \quad , \tag{72}$$

the group velocity being equal to

$$V = \frac{\left[1 + \left(p_3^{'} \right)^2 \right]^{1/2}}{\left| p_3 - p_1 \, p_3^{'} \right|} \tag{73}$$

Appendix C. Geometrical spreading in a VTI medium

We consider a ray from $\mathbf{x^s}$ to $\mathbf{x^r}$ in a VTI medium where the symmetry axis is parallel to the x_3-axis. From Appendix A in Schleicher et al. (2001) we obtain that

$$B_{ij}^{-1} \left(\mathbf{x^r}, \, \mathbf{x^s} \right) = - \left[\frac{\partial^2 T \left(\mathbf{x^r}, \, \mathbf{x^s} \right)}{\partial x_i^s \, \partial x_j^r} \right] \qquad (i, \, j = 1, \, 2) \tag{74}$$

can be expressed by

$$\mathbf{B}^{-1} \left(\mathbf{x^r}, \, \mathbf{x^s} \right) = \begin{bmatrix} \cos \alpha^s & 0 \\ 0 & 1 \end{bmatrix} \mathbf{Q_2^{-1}} \left(\mathbf{x^r}, \, \mathbf{x^s} \right) \begin{bmatrix} \cos \alpha^r & 0 \\ 0 & 1 \end{bmatrix} \tag{75}$$

where α^r and α^s are the angles the ray makes with the symmetry axis. From Appendix A in Ursin & Hokstad (2003), we have

$$\mathbf{B}^{-1} = \begin{bmatrix} \frac{\partial^2 T}{\partial r^2} & 0 \\ 0 & \frac{1}{r} \, \frac{\partial T}{\partial r} \end{bmatrix} \tag{76}$$

where r is the horizontal distance between the source and the receiver. Here, $r = x_1$, and with $p_1 = {}^{dT}/_{dx_1}$ and Eq.(68) the result is

$$\mathbf{B} = \begin{bmatrix} \frac{dx_1}{dp_1} & 0 \\ 0 & \frac{x_1}{p_1} \end{bmatrix} = -x_3 \begin{bmatrix} p_3'' & 0 \\ 0 & \frac{p_3'}{p_1} \end{bmatrix} \tag{77}$$

Eq.(75) gives

$$\mathbf{Q_2}^{-1}(\mathbf{x^r}, \mathbf{x^s}) = \begin{bmatrix} \frac{1}{\cos\,\alpha^s} & 0 \\ 0 & 1 \end{bmatrix} \mathbf{B}^{-1} \begin{bmatrix} \frac{1}{\cos\,\alpha^r} & 0 \\ 0 & 1 \end{bmatrix} \tag{78}$$

and

$$\mathbf{Q_2}(\mathbf{x^r}, \mathbf{x^s}) = \begin{bmatrix} \cos\,\alpha^r & 0 \\ 0 & 1 \end{bmatrix} \mathbf{B} \begin{bmatrix} \cos\,\alpha^s & 0 \\ 0 & 1 \end{bmatrix} \tag{79}$$